

Spinning-black-hole binaries: The orbital hang up

M. Campanelli, C. O. Lousto, and Y. Zlochower

*Department of Physics and Astronomy, and Center for Gravitational Wave Astronomy,
The University of Texas at Brownsville, Brownsville, Texas 78520*

(Dated: November 7, 2018)

We present the first fully-nonlinear numerical study of the dynamics of highly spinning black-hole binaries. We evolve binaries from quasicircular orbits (as inferred from Post-Newtonian theory), and find that the last stages of the orbital motion of black-hole binaries are profoundly affected by their individual spins. In order to cleanly display its effects, we consider two equal mass holes with individual spin parameters $S/m^2 = 0.757$, both aligned and anti-aligned with the orbital angular momentum (and compare with the spinless case), and with an initial orbital period of $125M$. We find that the aligned case completes three orbits and merges significantly after the anti-aligned case, which completes less than one orbit. The total energy radiated for the former case is $\approx 7\%$ while for the latter it is only $\approx 2\%$. The final Kerr hole remnants have rotation parameters $a/M = 0.89$ and $a/M = 0.44$ respectively, showing the unlikelihood of creating a maximally rotating black hole out of the merger of two spinning holes.

PACS numbers: 04.25.Dm, 04.25.Nx, 04.30.Db, 04.70.Bw

I. INTRODUCTION

Spinning black holes play an important role in some of the most energetic astrophysical phenomena in the universe. They form part of the main engine of gamma-ray bursts, being much more efficient at converting matter into radiation than non-spinning black holes. They are also responsible for the radio jets observed in active galactic nuclei, and the merger of two non-aligned spinning black holes is the likely explanation for the rapid directional changes observed in these jets when galaxies collide [1]. Recent estimates [2] of the spin of stellar mass black holes by spectral fitting of the X-Ray continuum set the rotation parameter of two dynamically confirmed black holes at $a/M \sim 0.75$. Accretion, of course, can spin up black holes, reaching up to a sub-maximal spin rate of $a/M \sim 0.95$, when magneto-hydrodynamics is taken into account [3, 4]. Other models using the combined effects of gas accretion and binary-black-hole coalescence suggest that black holes may be rapidly rotating in all epochs [5].

Recently new numerical techniques to solve the field equations of General Relativity have been developed [6, 7, 8, 9, 10] that make it possible to stably evolve black-hole binaries for several orbits and to compute the corresponding gravitational waveforms [11, 12, 13]. Numerical simulations of unequal-mass black-hole binaries, along with the calculation of the merger kicks, have been reported in Refs [14, 15, 16]. While research has been mainly focused on initially non-spinning black holes, there are important questions to be addressed when we consider highly-spinning black holes (see [17] and references therein).

In this paper we study how the emission of gravitational radiation affects the orbital trajectory of highly-spinning, equal-mass black holes as a function of the spin orientation. In order to maximize the effect, we

consider black-hole binaries with both spins aligned and anti-aligned with the orbital angular momentum, as well as the corresponding spinless case. We shall consider quasicircular orbit initial data with the same initial orbital period (as determined by the third post-Newtonian (3PN) expansion). In this way differences in the subsequent evolution can be attributed to the differences in the generation and emission of gravitational radiation.

In Ref. [18] the numerical evolutions of spinning binaries were studied for relatively modest values of the spins ($-0.25 \leq S/m^2 \leq 0.17$, m being the horizon mass of the individual holes) using the ‘Lazarus’ technique of matching full numerical evolutions to perturbation theory. In those evolutions the spin of the remnant Kerr hole increased with S/M^2 for the aligned case. Extrapolation to maximally spinning individual holes indicated that the remnant would remain sub-maximal for $S/m^2 < 0.85$. We will revisit this scenario, now reaching much higher values of the individual spins in order to make a more accurate statement.

II. INITIAL DATA

We use the Brandt-Brügmann puncture approach along with the elliptic solver BAM_Elliptic [19, 20] to compute initial data. Table I gives our choice of initial parameters. We have taken a fiducial angular frequency of $M\Omega = 0.05$, which corresponds to an orbital period of approximately $T = 125M$. This, accordingly to our previous simulation for non-spinning black holes [11] makes the binary complete more than a full orbit before the black holes merge. We choose individual spins $S = \pm 0.757 m^2$ (as measured using isolated horizon techniques [21]) to guarantee that the total angular momentum in the aligned case exceeds M^2 , the maximum allowed value for a common horizon to form. The gravita-

TABLE I: Initial data for quasicircular orbits of black-hole binaries with spin. The holes have proper horizon separation l , with puncture locations $(0, \pm y, 0)$, linear momenta $(\mp P, 0, 0)$, and spin $(0, 0, S)$. J is the total angular momentum, L is the orbital angular momentum, Ω is the orbital frequency, m_p is the individual puncture mass. All in units of the ADM mass M .

S/m^2	++0.757	0.00	--0.757
l/M	9.27	9.62	10.34
y/M	3.0595	3.280	3.465
P/M	0.1291	0.1336	0.1382
S/M^2	+0.1939	0.000	-0.1924
J/M^2	1.1778	0.8764	0.5729
L/M^2	0.7900	0.8764	0.9577
$M\Omega$	0.0500	0.0500	0.0500
m_p/M	0.3344	0.4851	0.3344

tional radiation emitted should efficiently carry out angular momentum from the system in order for the *cosmic censorship* conjecture to hold [22]. We can thus begin to explore its validity here, and this will be the subject of a more detailed study in a forthcoming paper by the authors.

With our choices of the spins and the orbital angular frequency, we determine the remaining orbital parameters by imposing quasicircular orbits according to the second post-Newtonian expansion of spinning particles [23] extended by the third-order orbital corrections [24]. We then give those parameters to the exact Bowen [25] solution of the momentum constraints and solve for the conformal factor of the (conformally flat) three-metric to complete our choice of the initial data. This post-Newtonian data should produce orbits with acceptably small eccentricities, as can be seen when comparing the zero-spin parameters in table I with others proposed in the literature (e.g. [26]). We have also briefly studied the effects of a different choice of the form of the initial data (Kerr conformal extrinsic curvature) for spinning black holes, as proposed in Ref. [27]. However, the spurious radiation in the initial data is dominated by the momentum terms and both data sets give nearly identical waveforms (see Fig. 3).

III. TECHNIQUES

We evolved these black-hole-binary data sets using the *LazEv* [28] implementation of the moving puncture approach [9, 10]. In our version of the moving puncture approach [9] we replace the BSSN [29, 30, 31] conformal exponent ϕ , which is infinite on the punctures, with the initially C^4 field $\chi = \exp(-4\phi)$. This new variable, along with the other BSSN variables, will remain finite provided that one uses a suitable choice for the gauge.

We obtained accurate, convergent waveforms by evolving this system in conjunction with a modified 1+log lapse, a modified Gamma-driver shift condition [9, 32],

and an initial lapse $\alpha \sim \psi_{BL}^{-4}$. The lapse and shift are evolved with $(\partial_t - \beta^i \partial_i)\alpha = -2\alpha K$, $\partial_t \beta^a = B^a$, and $\partial_t B^a = 3/4 \partial_t \tilde{\Gamma}^a - \eta B^a$. These gauge conditions require careful treatment of χ near the puncture in order for the system to remain stable [9, 11]. For our version of the moving puncture approach, we find that the product $\alpha \tilde{A}^{ij} \partial_j \phi$ has to be initially C^4 on the puncture. In the spinning case, \tilde{A}^{ij} is $O(r^3)$ on the puncture, thus requiring that $\alpha \propto r^3$ to maintain differentiability. We therefore choose an initial lapse $\alpha \sim \psi_{BL}^{-4}$ (which is $O(r^4)$ and C^4 on the puncture). In particular, $\alpha(t=0) = 2/(1 + \psi_{BL}^4)$ reproduces the isotropic Schwarzschild lapse at large distances from the hole. The initial values of β^i and B^i were set to zero.

The minimum resolution required to accurately model the dynamics of the merger scales with m_p . We would expect satisfactory results for a minimum resolution of $h = M/30$ (based on the non-spinning case, where satisfactory results were obtained with $h = M/21$, and the ratio of the puncture masses in the spinning and non-spinning cases), M being the total ADM mass. However, the additional power of $1/r$ introduced to K_{ij} because of spin, necessitates even higher resolution (we estimate $M/40 - M/50$) to get highly accurate waveforms.

We exploited the Pi-rotational symmetry about the z -axis as well as the reflection symmetry about the xy plane to reduce the size of the computational domain by one quarter.

IV. RESULTS

We evolved the ‘--0.757’ configuration using grid sizes of $320^2 \times 640$, $384^2 \times 768$, and $448^2 \times 896$ and resolutions of $M/25$, $M/30$, and $M/35$ respectively. We used a multiple transition fisheye [11] to push the physical boundaries to $134M$. We calculate ψ_4 in the Quasi-Kinnersley frame using the recently developed techniques of Ref. [33] that allow a meaningful extraction closer to the hole. In Fig. 1 we show the real part of the $(\ell = 2, m = 2)$ mode of $r\psi_4$ for the --0.757 case (extracted at $r = 10M$) for these resolutions, as well as a convergence plot of these data. The waveforms show fourth-order convergence up to $t \sim 110M$. The phase error from the $h = M/25$ run becomes too large to measure a meaningful convergence rate after $t \sim 110M$. Higher resolution runs will remain convergent, as demonstrated by the better phase agreement between the $M/30$ and $M/35$ runs. We extract the waveform at $10M$ to minimize the effects of the extreme fisheye deresolution (which is too strong in the far field to get accurate waveforms). After a time translation, the waveforms from the three runs only differ by a constant phase factor. We calculate this factor and plot the phase-corrected waveforms [12, 34] in the upper inset of Fig. 1. Note the near perfect agreement both in the orbital and plunge waveforms. The waveforms calculated at $r = 10M$ do not yield accurate estimates for the radiated energy (as expected, since the observer is still in

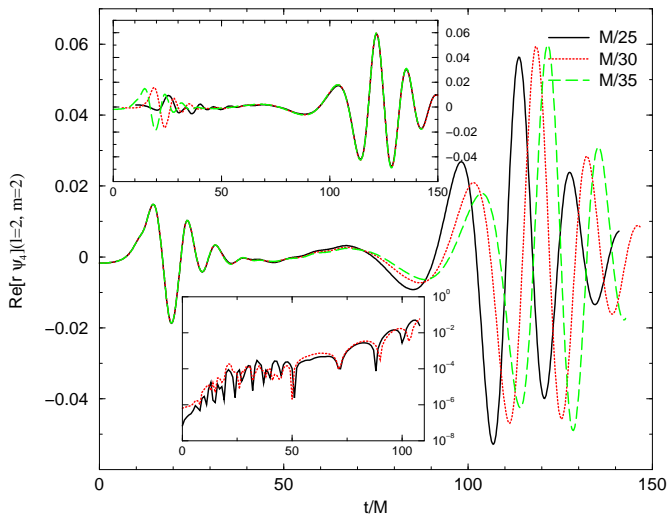


FIG. 1: The real ($\ell = 2, m = 2$) component of $r\psi_4$ in the Quasi-Kinnersley tetrad at $r = 10M$ for the $--0.757$ case. The lower inset shows the differences $r\psi_4(M/25) - r\psi_4(M/30)$ (solid line) and $r\psi_4(M/30) - r\psi_4(M/35)$ (dotted line), the latter rescaled by 2.33 to demonstrate fourth-order convergence. The lack of convergence for $t < 10M$ is due to roundoff effects in the initial data solver. The upper inset shows the real part of the phase-corrected ($\ell = 2, m = 2$) mode of ψ_4 at the same radius. Note the near-perfect agreement after $t = 45M$.

the near zone). However, as shown below, we obtained highly accurate estimates for the radiation by examining the remnant horizon. In order to obtain accurate measurements for the radiated energy and angular momentum from the waveform, one needs to use a weaker fisheye deresolution in the outer region, and carefully adjust the gauge so that the waveform is highly accurate at large radii ($r \sim 50M$).

The relatively large phase errors in this spinning case compared with our zero-spin simulations [11] are due to the fact that the effective resolution in the spinning case is smaller due to the smaller value of m_p as well as the lower order differentiability of the spinning data compared to zero-spin. A likely explanation is that numerical dissipation (which more strongly affects this higher frequency data) causes the merger to happen sooner than expected. This dissipation decreases with resolution.

We used Jonathan Thornburg’s AHFinderDirect thorn [35] to calculate the apparent horizons. We find that the common horizon is first detected at $t = 105.5M$ and has a mass of $M_{\mathcal{H}} = 0.978 \pm .001M$ and rotation parameter of $a/M_{\mathcal{H}} = 0.443 \pm 0.001$. During the merger ($2.2 \pm 0.1\%$) of the mass and ($26 \pm 2\%$) of the angular momentum are converted into radiation.

$M_{\mathcal{H}}$ and $a/M_{\mathcal{H}}$ were obtained from the asymptotic values of the horizon surface area and the ratio of the polar to equatorial circumferences (see Refs [9, 35, 36]). The ranges given for these quantities arise from the uncertainties in obtaining these values at finite time, and are

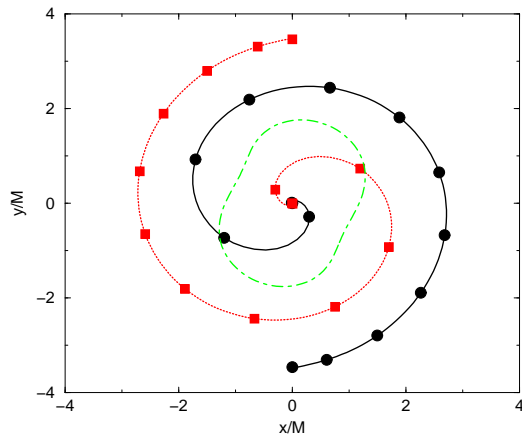


FIG. 2: The puncture trajectories on the xy plane for the $--$ case with resolution $M/35$. The spirals are the puncture trajectories with ticks every $10M$ of evolution. The dot-dash ‘peanut shaped’ figure is the first detected common horizon at $105.5M$. The (extrapolated) period of the last orbit is around $120M$.

independent of resolution. Thus, these horizon parameters give an accurate and robust measurement (even in the unresolved $h = M/25$ case) for the radiated mass and angular momentum.

Figure 2 shows the trajectories of the punctures for the $--0.757$ configuration as well as the projection of the first common horizon on the xy plane. It is evident from the waveform and the track that the binary undergoes ~ 0.9 orbits before merging.

We evolved the $++$ configuration with a grid size of $384^2 \times 768$ and resolution of $M/30$. We used multiple transition fisheye to push the boundaries to $159M$. In Fig. 3 we show the ($\ell = 2, m = 2$) mode of $r\psi_4$ in the Quasi-Kinnersley frame for the $++0.757$ case, again extracted at $r = 10M$. Note the ‘plunge’ waveform is delayed by $\sim 120M$ compared to the $--0.757$ case. The waveform shows approximately six periods of orbital radiation prior to the plunge waveform, indicating that the binary completed approximately three orbits.

We repeated the $++0.757$ case with a gridsizes of $448^2 \times 896$ and resolution of $M/30$ to force the boundaries to $266M$. This new configuration allows us to accurately obtain the horizon parameters (since they are not contaminated by the boundary), but is too coarse in the far-field region to produce accurate waveforms. The first common horizon was detected at $t = 232.5M$. In this case the final horizon had a mass of $0.933 \pm .001M$ and spin of $0.890 \pm .002$ (indicating that $(6.7 \pm 0.2\%)$ of the mass and $(34 \pm 1\%)$ of the angular momentum are radiated away). Table II gives a summary of these results. Note that the above values for the radiated energy are in rough agreement with those estimated using the effective one body approximation for maximally spinning holes [37].

Figure 4 shows the track for the $++0.757$ configura-

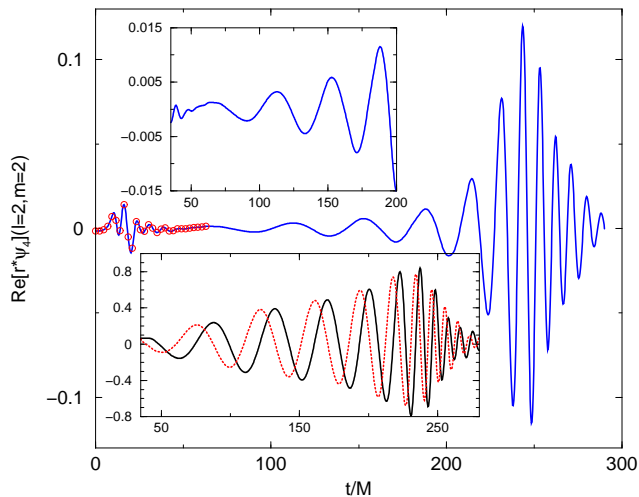


FIG. 3: The real part of the ($\ell = 2, m = 2$) mode of $r\psi_4$ in the Quasi-Kinnersley frame at $r = 10M$ from the ‘++0.757’ configuration. (The small circles are the early-time waveform from conformal Kerr data.) The top inset shows a magnified view of the early orbital motion. Note that the ‘++0.757’ waveform has 6 wavelengths of orbital motion prior to the plunge waveform (at $t \sim 232.5M$), indicating that the binary orbited approximately three times before merging. The bottom inset shows the real (solid) and imaginary (dotted) components of the (2,2) component of the strain h calculated at $r = 10M$.

tion. Note that the spiral is much tighter than in the ‘--0.757’ configuration, and that the binary completes roughly 3 orbits before the common horizon forms. Note also that the first common horizon is much smaller in this case (in these coordinates) than in the ‘--0.757’ case.

To demonstrate consistency with the General Relativity field equations, we calculated the Hamiltonian constraint violation. The constraint converges to fourth-order outside a small region surrounding the puncture (the constraint violation on the nearest neighboring points to the puncture is roughly independent of resolution, but this non-converging error does not propagate outside the individual horizons). Figure 5 shows the Hamiltonian constraint violations for the ‘--’ configuration along the x -axes at $t = 45M$ and along the y -axis at $t = 80M$ (at the time when the punctures cross the x -axis and $5M$ after the punctures cross the y -axis for the second time) for the $M/30$ and $M/35$ runs. The constraint is convergent everywhere except points contaminated by boundary errors (these points have been removed from the plot) and at the points closest to the puncture.

We complete our initial study with the corresponding spinless case as a reference point. For details on the accuracy and evolution of the spinless case see Ref. [11]. We evolved the zero-spin case with a resolution of $M/22.5$ and gridsize of $320^2 \times 640$ (the outer boundary was located at $216M$). The first common horizon formed at $t = 161M$ with mass $(0.965 \pm .001)\%$ and spin $a/M =$

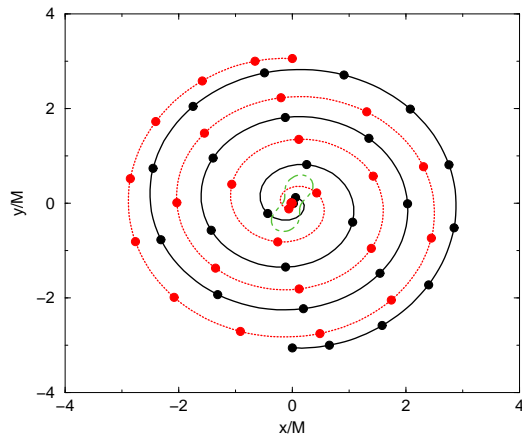


FIG. 4: The puncture trajectories on the xy plane for ‘++’ configuration with resolution $M/30$. The spirals are the puncture trajectories with ticks every 10M of evolution. The dot-dash ‘peanut shaped’ figure is the first detected common horizon at $t = 232.5M$. The period of the last orbit is around $36M$. The last orbit begins when the punctures are located at $1.4M$ from the origin (in these coordinates).

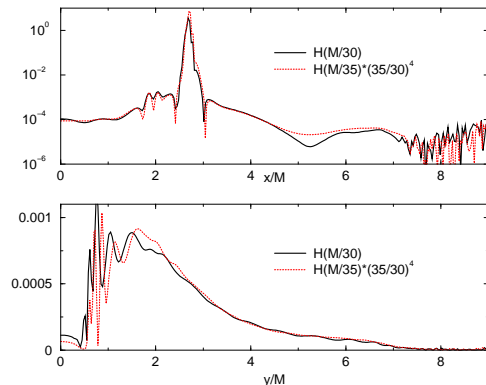


FIG. 5: The Hamiltonian constraint violation at $t = 45M$ along the x -axis (top plot) and at $t = 80M$ along the y -axis (bottom plot) for the $M/30$ and $M/35$ runs (the latter rescaled by $(35/30)^4$) for the ‘--’ configuration. The punctures crossed the x -axis at $t = 45M$ and crossed the y -axis for the second time at $t = 75M$. Note the reasonable fourth-order convergence (except at the puncture). Points contaminated by boundary errors have been excluded from the plot. The high frequency violations near the numerical coordinate $y/M = \pm 9$ are due to the extreme fisheye deresolution near the boundary, and converge with resolution.

$(0.688 \pm .001)$. This corresponds to a radiated energy and angular momentum of $(3.5 \pm 0.1)\%$ and $(26.9 \pm 0.1)\%$ respectively.

TABLE II: Results of the evolution as determined from the remnant horizons. The horizon formed at $t = 224.5M$ for the ‘++0.757’ configuration, $t = 105.5M$ for the ‘--0.757’ configuration, and $t = 161M$ for the spinless configuration.

S/m^2	E_{rad}/M_{ADM}	J_{rad}/J_{ADM}	$a/M_{\mathcal{H}}$
++0.757	$(6.7 \pm 0.2)\%$	$(34 \pm 1)\%$	0.890 ± 0.002
--0.757	$(2.2 \pm 0.1)\%$	$(26 \pm 2)\%$	0.443 ± 0.001
0.00	$(3.5 \pm .1)\%$	$(26.9 \pm 0.1)\%$	0.688 ± 0.001

V. DISCUSSION

In this paper we have shown that the ‘moving puncture’ approach can be used to accurately simulate the inspiral orbit of spinning-black-hole binaries. We found that the spin-orbit coupling delays the onset of the plunge phase (compared to the non-spinning case) when the spins are aligned with the orbital angular momentum, while in the anti-aligned case the plunge phase is hastened. In all cases, the black holes merge to form a single Kerr black hole with rotation parameter $a/M < 1$.

A fit of the remnant spin to the spins of the initial black holes leads to the simple extrapolation formula $a/M \approx 0.688 + 0.298(S/m^2) - 0.038(S/m^2)^2$. Although more accurate simulations are needed, these results show that it is very unlikely to form a nearly maximally rotating black hole out of the merger of two highly spinning ones. Our results reinforce the same qualitative conclusions reached with the Lazarus approach [18], and are consistent with those in Refs [17, 37]. Extrapolation of the radiated energy to maximally rotating black holes with the fit $E_{rad}/M \approx 3.5 + 3(S/m^2) + 152/90(S/m^2)^2$ set it near 8.2%, not far from the assumed 10% in Ref. [17] a decade ago.

For the ‘--0.757’ case the final orbit lasts $\sim 120M$ starting at a separation of $7M$ in coordinate space, while for the ‘++0.757’ case we have found that the duration of the last orbit is $\sim 36M$ at a coordinate separation of $2.8M$. It is worth noting from [38], that the orbital period associated with the ISCO for the ‘++0.17’ case

is roughly $27M$ at a coordinate separation of $1.6M$, and that no ISCO was found for higher spin configurations. This highlights again the importance of the gravitational radiation in the late binary black hole dynamics which is not captured in the determinations of the ISCO. On the other hand, the dependence of the ISCO on spin correctly implies that the ‘++’ configurations are more stable at close separations than the ‘--’ configurations. This stability property is observed in the significantly tighter spiral displayed in Fig. 4.

The Post-Newtonian equations of motion [23] indicate that the leading spin-orbit interaction is of 1.5PN order, while the spin-spin interaction is of 2PN order. It is the spin-orbit interaction (attractive/repulsive for --/++ configurations respectively) responsible for the longer the stability of the aligned spin binary.

Many outstanding issues involving spinning black hole scenarios remain to be explored. We plan to study some of them next, including additional values of the individual spins for the ‘++’ cases in order to better extrapolate the results to the limiting maximally rotating individual holes, as well as unaligned spins to study precessional effects. Finally, more significant computer resources and the use of Adaptive Mesh Refinement techniques combined with higher order finite difference methods will be needed to achieve the accuracy required to aid gravitational wave detection efforts [39].

Acknowledgments

We thank Bernard Kelly for careful reading of this text. We thank Erik Schnetter for providing the Cactus thorns to implement Pi-symmetry boundary conditions. We thank the referee for helpful suggestions. We gratefully acknowledge the support of the NASA Center for Gravitational Wave Astronomy at University of Texas at Brownsville (NAG5-13396) and the NSF for financial support from grants PHY-0140326 and PHY-0354867. Computational resources were performed by the 70-node ‘Funes’ cluster at UTB.

-
- [1] D. Merritt and R. D. Ekers, *Science* **297**, 1310 (2002).
 - [2] R. Shafee et al., *Astrophys. J.* **636**, L113 (2006).
 - [3] S. L. Shapiro, *Astrophys. J.* **620**, 59 (2005).
 - [4] C. F. Gammie, S. L. Shapiro, and J. C. McKinney, *Astrophys. J.* **602**, 312 (2004).
 - [5] M. Volonteri, P. Madau, E. Quataert, and M. J. Rees, *Astrophys. J.* **620**, 69 (2005).
 - [6] B. Brügmann, W. Tichy, and N. Jansen, *Phys. Rev. Lett.* **92**, 211101 (2004).
 - [7] P. Diener et al., *Phys. Rev. Lett.* **96**, 121101 (2006).
 - [8] F. Pretorius, *Phys. Rev. Lett.* **95**, 121101 (2005).
 - [9] M. Campanelli, C. O. Lousto, P. Marronetti, and Y. Zlochower, *Phys. Rev. Lett.* **96**, 111101 (2006).
 - [10] J. G. Baker, J. Centrella, D.-I. Choi, M. Koppitz, and J. van Meter, *Phys. Rev. Lett.* **96**, 111102 (2006).
 - [11] M. Campanelli, C. O. Lousto, and Y. Zlochower, *Phys. Rev. D* **73**, 061501(R) (2006).
 - [12] J. G. Baker, J. Centrella, D.-I. Choi, M. Koppitz, and J. van Meter, *Phys. Rev. D* **73**, 104002 (2006).
 - [13] F. Pretorius (2006), gr-qc/0602115.
 - [14] M. Campanelli, *Class. Quant. Grav.* **22**, S387 (2005).
 - [15] F. Herrmann, D. Shoemaker, and P. Laguna (2006), gr-qc/0601026.
 - [16] J. G. Baker et al. (2006), astro-ph/0603204.
 - [17] Éanna É. Flanagan and S. A. Hughes, *Phys. Rev. D* **57**, 4535 (1998).
 - [18] J. Baker, M. Campanelli, C. O. Lousto, and R. Takahashi, *Phys. Rev. D* **69**, 027505 (2004).

- [19] S. Brandt and B. Brügmann, *Phys. Rev. Lett.* **78**, 3606 (1997).
- [20] <http://www.cactuscode.org>.
- [21] O. Dreyer, B. Krishnan, D. Shoemaker, and E. Schnetter, *Phys. Rev. D* **67**, 024018 (2002).
- [22] R. M. Wald, *General Relativity* (The University of Chicago Press, Chicago, 1984), ISBN 0-226-87032-4 (hardcover), 0-226-87033-2 (paperback).
- [23] L. E. Kidder, *Phys. Rev. D* **52**, 821 (1995).
- [24] L. Blanchet, *Pramana* **53**, 1 (1999).
- [25] J. M. Bowen, *Gen. Rel. Grav.* **11**, 227 (1979).
- [26] W. Tichy and B. Brügmann, *Phys. Rev. D* **69**, 024006 (2004).
- [27] S. Dain, C. O. Lousto, and R. Takahashi, *Phys. Rev. D* **65**, 104038 (2002).
- [28] Y. Zlochower, J. G. Baker, M. Campanelli, and C. O. Lousto, *Phys. Rev. D* **72**, 024021 (2005).
- [29] T. Nakamura, K. Oohara, and Y. Kojima, *Prog. Theor. Phys. Suppl.* **90**, 1 (1987).
- [30] M. Shibata and T. Nakamura, *Phys. Rev. D* **52**, 5428 (1995).
- [31] T. W. Baumgarte and S. L. Shapiro, *Phys. Rev. D* **59**, 024007 (1999).
- [32] M. Alcubierre, B. Brügmann, P. Diener, M. Koppitz, D. Pollney, E. Seidel, and R. Takahashi, *Phys. Rev. D* **67**, 084023 (2003).
- [33] M. Campanelli, B. Kelly, and C. O. Lousto, *Phys. Rev. D* **73**, 064005 (2006).
- [34] J. Baker, M. Campanelli, C. O. Lousto, and R. Takahashi, *Phys. Rev. D* **65**, 124012 (2002).
- [35] J. Thornburg, *Class. Quantum Grav.* **21**, 743 (2004).
- [36] M. Alcubierre et al., *Phys. Rev. D* **72**, 044004 (2005).
- [37] A. Buonanno, Y. Chen, and T. Damour (2005), [gr-qc/0508067](https://arxiv.org/abs/gr-qc/0508067).
- [38] H. P. Pfeiffer, S. A. Teukolsky, and G. B. Cook, *Phys. Rev. D* **62**, 104018 (2000).
- [39] M. Miller, *Phys. Rev. D* **71**, 104016 (2005).
-